Reduction of CuO and Cu₂O with H₂: H Embedding and Kinetic Effects in the Formation of Suboxides

Jae Y. Kim,[†] José A. Rodriguez,[*,†] Jonathan C. Hanson,[†] Anatoly I. Frenkel,[§] and Peter L. Lee[‡]

*Contribution from the Chemistry Department, Brookhaven National Laboratory,
Upton, New York 11973, Department of Physics, Yeshiva University,
New York, New York 10016, and Advanced Photon Source, Argonne National Laboratory,
Argonne, Illinois 60439*

Received March 13, 2003; E-mail: rodrigez@bnl.gov

Abstract: Time-resolved X-ray diffraction, X-ray absorption fine structure, and first-principles density functional calculations were used to investigate the reaction of CuO and Cu₂O with H₂ in detail. The mechanism for the reduction of CuO is complex, involving an induction period and the embedding of H into the bulk of the oxide. The in-situ experiments show that, under a normal supply of hydrogen, CuO reduces directly to metallic Cu without formation of an intermediate or suboxide (i.e., no Cu₄O₃ or Cu₂O). The reduction of CuO is easier than the reduction of Cu₂O. The apparent activation energy for the reduction of CuO is about 14.5 kcal/mol, while the value is 27.4 kcal/mol for Cu₂O. During the reduction of CuO, the system can reach metastable states (MS) and react with hydrogen instead of forming Cu₂O. To see the formation of Cu₂O, one has to limit the flow of hydrogen, slowing the rate of reduction to allow a MS → Cu₂O transformation. These results show the importance of kinetic effects for the formation of well-defined suboxides during a reduction process and the activation of oxide catalysts.

I. Introduction

Although the reduction of metal oxides using hydrogen is a frequently used method to prepare active catalysts and electronic devices,[1] the reduction process is generally not well understood at a molecular or atomic level.[2] Traditionally the process has been described using phenomenological models where the rate of reaction depends on the initial nucleation of the new phase (i.e., the reduced oxide) or on the area of the reduced-phase/oxide interface.[1b,2b,c] Recent studies illustrate the important role played by O vacancies in the mechanism for reduction of an oxide.[3] The phenomenological kinetic models frequently used in the description of the reduction process[1b,2b,c] can be useful, but a more relevant aspect is the initial production of active sites for the rapid dissociation of H₂.[3] This alone can lead to the appearance of "induction periods" in the reaction kinetics and the possibility for autocatalysis. In some cases, the situation can become even more complex due to the embedding of hydrogen into the lattice of the oxide before the reduction process starts.[4]

The controlled synthesis of well-defined suboxides through reduction in H₂ is a key issue in the activation of oxide catalysts.[1b,2b] In practical terms, one needs to know what are the kinetic and thermodynamic parameters that determine the formation of a suboxide.[1b,2b] At a fundamental level, one must understand the interplay among H₂ dissociation, oxygen removal (i.e., generation of O vacancies), and the relative stability of a suboxide. Copper oxide, an antiferroelectric semiconductor with a band gap of about 1.4 eV,[2a] is a benchmark system[1,2] which provides a sequential pathway for a change in oxidation of state from "+2" to 0 (CuO → Cu₄O₃ → Cu₂O → Cu). In this respect, Cu₄O₃ and Cu₂O are suboxides with well-known crystal structures.[5–7] Mixtures of CuOₓ/Cu are utilized for the fabrication of components in the microelectronic industry.[1a,8] CuO is used as a catalyst or catalyst precursor in many chemical reactions that involve hydrogen as a reactant or a product: methanol synthesis from CO (CO + 2H₂ ⇌ CH₃OH) or CO₂ (CO₂ + 3H₂ ⇌ CH₃OH + H₂O),[2b,9] the water-gas shift reaction (CO + H₂O ⇌ CO₂ + H₂),[10] methanol steam re-forming

---

† Brookhaven National Laboratory.
§ Yeshiva University.
‡ Argonne National Laboratory.

(1) (a) Li, J.; Mayer, J. W.; Tu, K. N. *Phys. Rev. B* **1992**, 45, 5683. (b) Delmon, B. In *Handbook of Heterogeneous Catalysis*; Ertl, G., Knözinger, H., Weitkamp, J., Eds.; Wiley-VCH: New York, 1997; pp 264−277.
(2) (a) Henrich, V. E.; Cox, P. A. *The Surface Science of Metal Oxides*; Cambridge University Press: Cambridge, U.K., 1994. (b) Kung, H. H. *Transition Metal Oxides: Surface Chemistry and Catalysis*; Elsevier: New York, 1989. (c) Delmon, B. *Introduction á la Cinétique Hétérogène*; Technip: Paris, 1969.
(3) Rodriguez, J. A.; Hanson, J. C.; Frenkel, A. I.; Kim, J. Y.; Pérez, M. *J. Am. Chem. Soc.* **2002**, *124*, 346.

(4) (a) Sohlberg, K.; Pantelides, S. K.; Pennycook, S. J. *J. Am. Chem. Soc.* **2001**, *123*, 6609. (b) Rodriguez, J. A.; Hanson, J. C.; Kim, J.-Y.; Liu, G. J.; Iglesias-Juez, A.; Fernández-García, M. *J. Phys. Chem. B* **2003**, 107, 3535.
(5) PDF # 33-0480, JCPDS Powder Diffraction File, Int. Center for Diffraction Data, Swarthmore, PA, 1989.
(6) PDF # 05-0667, JCPDS Powder Diffraction File, Int. Center for Diffraction Data, Swarthmore, PA, 1989.
(7) O'Keeffe, M.; Bovin, J.-O. *Am. Mineral.* **1978**, *63*, 180.
(8) Li, J.; Wang, S. Q.; Mayer, J. W.; Tu, K. N. *Phys. Rev. B* **1989**, 39, 12367, and references therein.
(9) (a) Klier, K. *Adv. Catal.* **1982**, 31, 243 (b) Li, J. L. Takeguchi, T.; Inui, T. *Appl. Catal. A* **1996**, 139, 97.
(10) Newsome, D. S. *Catal. Rev.-Sci. Eng.* **1980**, *21*, 275.

$(CH_3OH + H_2O \rightleftharpoons CO_2 + 3H_2)$,[11] oxidative methanol reforming $(CH_3OH + 1/4O_2 + 1/2H_2O \rightleftharpoons CO_2 + 5/2H_2)$,[12] NO reduction $(NO + H_2 \rightleftharpoons 1/2N_2 + H_2O)$,[2b,13] etc. For years, there has been a big controversy about the relative importance of Cu^+ and Cu^0 centers in several of these catalytic reactions.[2,9,12−15] The data reported in the literature do not agree in the mechanism for CuO reduction.[9,14] Experiments of H_2 temperature-programmed reduction (TPR) show that the reduction of CuO occurs in one, two, or even three steps.[16−18] X-ray absorption near-edge structure (XANES) spectroscopy points to the existence of Cu^+ as a transient species in the reduction of Cu^{2+} to Cu^0,[12,15,19] but such an intermediate was not detected in X-ray diffraction (XRD) measurements.[20] These discrepancies could be a consequence of the different conditions used in the reduction experiments, or they could originate from differences in the handling/preparation of the CuO samples. It is very important to examine the reduction of CuO with H_2 in situ, because for this system ex situ investigations may not represent the "real" state of the copper phase under reduction conditions.[12,15]

To the best of our knowledge, no systematic studies using in-situ X-ray diffraction have been reported for the reaction of H_2 with pure CuO and Cu_2O systems. Investigations at Brookhaven National Laboratory have established the feasibility of conducting subminute, time-resolved XRD experiments under a wide variety of temperature and pressure conditions $(-190\ °C < T < 900\ °C; P < 45\ \text{atm})$.[3,21] This important advance results from combining the high intensity of synchrotron radiation with rapid new parallel data-collection devices. In this work, time-resolved XRD was used to monitor chemical transformations and the long-range atomic order of the bulk copper oxides during reduction. Information about the short-range atomic order and local geometry of Cu was obtained by collecting data of X-ray absorption fine structure (XAFS), which was analyzed using the principal component analysis (PCA)[22−24] method. First-principles density-functional (DF) calculations[25] were used to examine the energetics of structural changes associated with the reduction process. Our results shed light into the controversial mechanism for CuO reduction and show the importance of kinetic effects for the generation of suboxides in this type of chemical process.

(11) Peppley, B. A.; Amphlett, J. C.; Kearns, L. M.; Mann, R. F. *Appl. Catal. A* **1999**, *179*, 31.
(12) Reitz, T. L.; Lee, P. L.; Czaplewski, K. F.; Lang, J. C.; Popp, K. E.; Kung, H. *J. Catal.* **2001**, *199*, 193.
(13) Dow, W.-P.; Huang, T.-J. *Appl. Catal. A* **1996**, *141*, 17.
(14) (a) Campbell, C. T. *Adv. Catal.* **1989**, *36*, 1. (b) Campbell, C. T.; Daube, K. A.; White, J. M. *Surf. Sci.* **1987**, *182*, 458. (c) Poulston, S.; Parlett, P. M.; Stone, P.; Bowker, M. *Surf. Interface Anal.* **1996**, *24*, 811. (d) van Kooten, W. E. J.; van Nispen, J. P. C.; Gijzeman, O. L. J.; Geus, J. W. *Appl. Surf. Sci.* **1995**, *90*, 137.
(15) Günther, M. M.; Ressler, T.; Jentoft, R. E.; Bems, B. *J. Catal.* **2001**, *203*, 133.
(16) Dow, W.-P.; Wang, Y.-P.; Huang, T. J. *J. Catal.* **1996**, *160*, 155.
(17) Dow, W.-P.; Huang, T. J. *Appl. Catal. A* **1996**, *141*, 17.
(18) Fernández-García, M.; Rodríguez-Ramos, I.; Ferreira-Aparicio, P.; Guerero-Ruiz, A. *J. Catal.* **1998**, *178*, 253.
(19) Neylon, M. K.; Marshall, C.; Kropf, J. To be published.
(20) Vong, M. S. W.; Sermon, P. A.; Grant, K. *Catal. Lett.* **1990**, *4*, 15.
(21) Norby, P.; Hanson, J. *Catal. Today* **1998**, 39, 301, and references therein.
(22) Diamantaras, K. I.; Kung, S. Y. *Principal Component Neural Networks: Theory and Applications*; John Wiley & Sons: New York, 1996.
(23) Wasserman, S. R. *J. Phys. IV* **1997**, *7*, C2−203.
(24) Frenkel, A. I.; Kleifeld, O.; Wasserman, S.; Sagi, I. *J. Chem. Phys.* **2002**, *116*, 9449.
(25) Payne, M. C.; Allan, D. C.; Arias, T. A.; Johannopoulos, J. D. *Rev. Mod. Phys.* **1992**, *64*, 1045.

II. Experimental and Theoretical Methods

(i) XRD Measurements. The time-resolved X-ray diffraction data were collected in the temperature range 150−300 °C at the beamline X7B ($\lambda = 0.9034$ Å) of the National Synchrotron Light Source (NSLS) in Brookhaven National Laboratory (BNL) using a MAR345 area detector. The XRD diffraction data with a high-order wave vector Q (≈ 11.5 Å^{-1}) were obtained at the beamline 1-ID ($\lambda = 0.1536$ Å) of X-ray Operation and Research in the Advanced Photon Source (APS) at Argonne National Laboratory. An identical setup system was employed for the experiments.[3,26] The powders of CuO and Cu_2O were obtained from commercial sources (>99.99% purity). Samples were loaded in an open sapphire capillary having an inner diameter of 0.5 mm. To keep the sample position constant from the gas flowing, quartz wools were added on each side of the powder. One end of the capillary was connected to an inlet with a 5% H_2 (99.9999% purity) and 95% He (99.9999% purity) gas mixture, and the other end was connected to a meter to monitor the gas flow rate constant (flow rate $\approx 5-15$ cm^3/min). A residual gas analyzer (RGA) was also attached at the end of the flow meter to examine the products after the reaction.

A small resistance heater was designed by winding a kanthal wire around the sapphire capillary that contained the sample. A thermocouple was inserted into the capillary near the powder to maintain an accurate temperature throughout the measurements. Prior to collecting data from CuO and Cu_2O samples, a coefficient of thermal expansion from Y_2O_3 powder was measured from the same setup to calibrate the actual sample temperature by reported values.[27] The result showed a good agreement with the desired and measured sample temperatures. From the XRD data, occupancies of atoms, accurate lattice constants, and the concentration of phases appearing during the reaction were determined by a Rietveld analysis[28] using the GSAS (general structure analysis system) program.[29]

(ii) XANES/EXAFS Measurements. The time-resolved X-ray absorption measurements were performed at the beamline X16C of the NSLS at BNL using a setup nearly identical to that of our previous time-resolved studies.[3,30,31] The fine CuO and Cu_2O powders were uniformly spread with a brush over adhesive Kapton polyamide tape. Kapton is relatively transparent for X-rays at the 9−10 keV energy range, does not decompose at temperatures up to 400 °C, and thus makes a good support. The samples were then loaded into a custom-designed and -built catalysis cell and exposed to a flow of a 5% H_2 and 95% He gas mixture (15−20 cm^3/min) while the XANES or extended X-ray absorption fine structure (EXAFS) measurements were taken repetitiously during reaction at 250, 280, or 300 °C. The absorption edge steps, measured in transmission, in all the samples were ca. 0.2−0.25 at the Cu K absorption edge (8978 eV). The temperature was monitored with a chromel/alumel thermocouple mounted directly on the sample stage. At 300 and 280 °C, a total of 20−30 XANES scans (2.5 m per scan) were taken from 100 eV below the Cu K-edge to 200 eV above. At 250 °C, full EXAFS scans, from 150 eV below the Cu K-edge to 800 eV above, were measured 15 times, each scan lasting 14.5 m. The start of the first scan at each temperature was synchronized with the beginning of H_2 flow, and the data were taken until the difference between the successive spectra became smaller than the statistical noise in the data.

(ii) First-Principles Density Functional Calculations. In section III.3, density-functional (DF) calculations with the CASTEP (Cambridge

(26) Chupas, P. J.; Ciraolo, M. F.; Hanson, J. C.; Grey, C. P. *J. Am. Chem. Soc.* **2001**, *123*, 1694.
(27) *Thermophysical Properties of Matter*, Vol. 13: Thermal Expansion−Nonmetallic Solids.
(28) Rietveld, H. M. *J. Appl. Crystallogr.* **1969**, *2*, 65.
(29) Larson, A. C.; Von Dreele, R. B. Los Alamos National Lab. Report No. LAUR 86-748, 1994 (unpublished).
(30) Frenkel, A. I.; Hills, C. W.; Nuzzo, R. G. *J. Phys. Chem. B* **2001**, *105*, 12689.
(31) Nashner, M. S.; Frenkel, A. I.; Somerville, D.; Hills, C. W.; Shapley, J. R.; Nuzzo, R. G. *J. Am. Chem. Soc.* **1998**, *120*, 8093.

Serial Total Energy Package) suite of programs[25,32] are used to investigate the structure and stability of a series of copper oxides: CuO, CuO (25% of O vacancies), Cu_4O_3, CuO (50% of O vacancies), and Cu_2O. In this code, the Kohn–Sham implementation of DF theory is used to obtain the total energy of the system. CASTEP has an excellent track record in accurate prediction of geometry and energetics for inorganic compounds.[3,32–37] In this code, the wave functions of valence electrons are expanded in a plane wave basis set with k-vectors within a specified energy cutoff E_{cut}. Tightly bound core electrons are represented by nonlocal ultrasoft pseudopotentials.[38] Brillouin zone integration is approximated by a sum over special k-points chosen using the Monkhorst–Pack scheme.[39] In all the calculations, the kinetic energy cutoff E_{cut} (400 eV) and the density of the Monkhorst–Pack k-point mesh were chosen sufficiently high to ensure convergence of the computed structures and electronic properties. The exchange–correlation contribution to the total electronic energy was treated in a generalized gradient-corrected (GGA) form of the local density approximation (LDA): Perdew–Burke–Ernzerhoff functional.[40] The structural parameters of the bulk oxides in their different configurations were determined using the Broyden–Fletcher–Goldfarb–Shanno (BFGS) minimization technique, with the following thresholds for the converged structures: energy change per atom less than 5×10^{-6} eV, residual force less than 0.02 eV/Å, displacement of atoms during the geometry optimization less than 0.001 Å, and rms of the stress tensor less than 0.1 GPa. For each optimized structure, the partial charges on the atoms were estimated by projecting the occupied one-electron eigenstates onto a localized basis set with a subsequent Mulliken population analysis.[41,42] Mulliken charges have well-known limitations,[43] but are nevertheless useful as a qualitative tool to study trends in charge distribution.

III. Results

III.1. Time-Resolved XRD Studies. (i) Reduction of Cu_2O Powder. Before dealing with the reaction between H_2 and CuO, Cu_2O powders were first reduced to obtain reference information for the Cu_2O phase on peak shape, location, and behavior during reaction. In typical TPR experiments, oxides are heated under a temperature ramp in a hydrogen environment.[16–18] Time-resolved XRD results for the heating (rate 20 °C/min) of Cu_2O under a flow of 5% H_2/95% He show that the oxide starts to reduce near 300 °C and becomes metallic Cu upon further heating (Figure 1a). No intermediate phase is observed during the reduction (i.e., direct transformation from Cu^+ to Cu^0). In these experiments, the desorption of water was detected with a mass spectrometer at temperatures between 300 and 400 °C.

Since the TPR method does not allow a careful determination of the onset temperature for reduction and in some cases makes difficult the generation of intermediate compounds, isothermal reduction experiments were performed. Reduction behaviors at
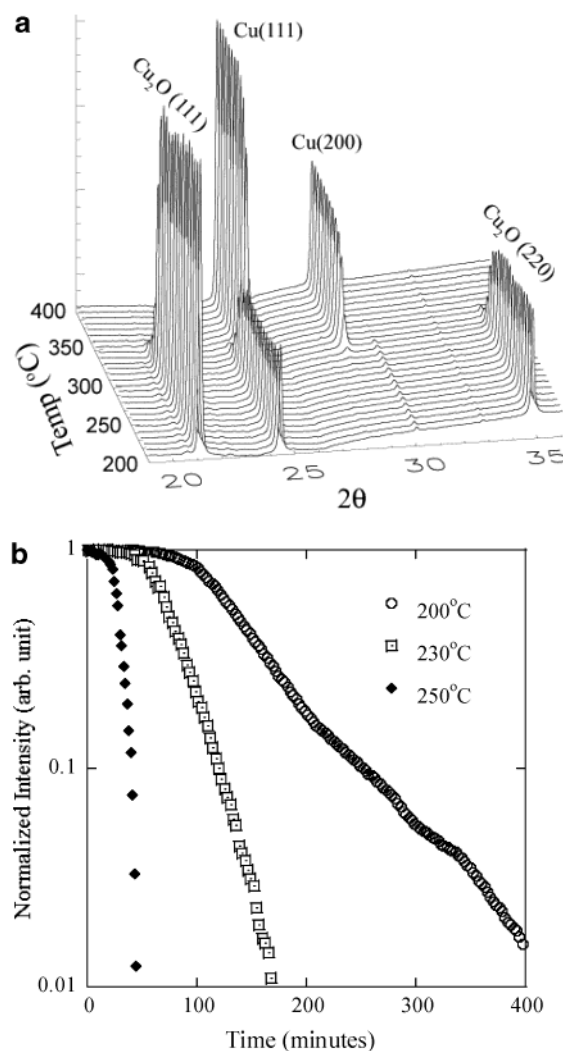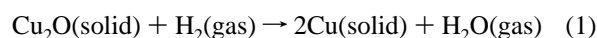
(32) Milman, V.; Winkler, B.; White, J. A.; Pickard, C. J.; Payne, M. C.; Akhmatskaya, E. V.; Nobes, R. H. *Int. J. Quantum Chem.* **2000**, *77*, 895.
(33) (a) Rodriguez, J. A.; Etxeberria, A.; González, L.; Maiti, A *J. Chem. Phys.* **2002**, *117*, 2699. (b) Rodriguez, J. A.; García, J.; González, L. *Chem. Phys. Lett.* **2002**, *365*, 380.
(34) Sorescu, D. C.; Yates, J. T. *J. Phys. Chem. B* **1998**, *102*, 4556.
(35) Rodriguez, J. A.; Maiti, A. *J. Phys. Chem. B* **2000**, *104*, 3630.
(36) Refson, K.; Wogelius, R. A.; Fraser, D. G.; Payne, M. C.; Lee, M. H.; Milman, V. *Phys. Rev. B* **1995**, *52*, 10823.
(37) Rodriguez, J. A.; Jirsak, T.; Pérez, M.; Chaturvedi, S.; Kuhn, M.; González, L.; Maiti, A. *J. Am. Chem. Soc.* **2000**, *122*, 12362.
(38) Vanderbilt, D. *Phys. Rev. B* **1990**, *41*, 7892.
(39) Monkhorst, H. J.; Pack, J. D. *Phys. Rev. B* **1976**, *13*, 5188.
(40) Perdew, J. P.; Burke, K.; Ernzerhof, M. *Phys. Rev. Lett.* **1996**, *77*, 3865.
(41) Segall, M. D.; Pickard, C. J.; Shah, R.; Payne, M. C. *Phys. Rev. B* **1996**, *54*, 16317.
(42) Segall, M. D.; Pickard, C. J.; Shah, R.; Payne, M. C. *Mol. Phys.* **1996**, *89*, 571.
(43) (a) Szabo, A.; Ostlund, N. S. *Modern Quantum Chemistry*; McGraw-Hill: New York, 1989. Wiberg, K. B.; Rablen, P. R. *J. Comput. Chem.* **1993**, *14*, 1504.

Figure 1. Synchrotron-based time-resolved in-situ XRD patterns ($\lambda = 0.9147$ Å) during the reduction of Cu_2O by H_2 at variable temperature, 200–400 °C (a), and peak intensity plots of the Cu_2O (111) peak as a function of time at different isothermal temperatures (b). The samples were exposed to a 5% H_2/ 95% He gas mixture (15–20 cm³/min flow).

isothermal conditions were similar to the ones determined by TPR means (no presence of an intermediate phase). In addition, an induction period for reaction was observed as shown in Figure 1b. This figure represents the change for the intensity of the Cu_2O phase as a function of time at isothermal conditions in the temperature range 200–250 °C. The induction period becomes shorter and the reduction rate gets faster when increasing the isothermal temperature: at 230 °C, for example, the powder starts to reduce after about 60 min and the reduction process completes in 180 min, while they are 100 and 450 min, respectively, at 200 °C. It is worthy to note that ~10% of the peak intensity decays during the induction time, indicating that a minor reduction already progresses during this period. At this stage, sites are probably being formed that have a high efficiency for the adsorption and dissociation of H_2.[3] Once a large supply of hydrogen is available on/in the oxide sample, the removal of oxygen as water (detected in mass spectroscopy) becomes faster:

$$Cu_2O(solid) + H_2(gas) \rightarrow 2Cu(solid) + H_2O(gas) \quad (1)$$

At the end of the reduction process, this removal of O is difficult. In some cases, not all Cu_2O powders completely reduce to a metallic Cu leaving a residue of the starting phase peak even at long exposure to H_2 (>60 min). Probably, some Cu_2O grains are coated by a fast reduced Cu film, leaving oxygen trapped.

In our experiments, the water formed by reaction 1 was removed from the system, preventing an equilibrium between the Cu_2O and Cu phases.[44] If the formed water is retained (i.e., closed system instead of a flow reaction cell), then Cu_2O and Cu could coexist in equilibrium.[44b]

(ii) Reduction of CuO Powder. The CuO system exhibits quite interesting behavior during the reduction process. First, our TPR results indicate that CuO powder starts to reduce near 280 °C under hydrogen flowing, which is slightly (about 20 °C) lower than the corresponding temperature found for Cu_2O. Second, time-resolved in-situ XRD patterns show that the formation of an intermediate phase depends strongly on the reaction conditions. Under the normal conditions of most catalytic processes (i.e., substantial pressures of hydrogen), a direct transformation from Cu^{2+} to Cu^0 occurs:

$$CuO(solid) + H_2(gas) \rightarrow Cu(solid) + H_2O(gas) \quad (2)$$
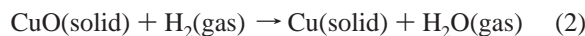
As shown in Figure 2a, CuO powders reduce to metallic Cu at 200 °C under a 5% H_2/95% He gas mixture (flow rate >15 cm^3/min). There is no hint of an intermediate phase, Cu_4O_3 or Cu_2O,[5-7] during the reduction. Instead, diffraction peaks for Cu appear and increase their intensity as the CuO peaks become weaker. A representative plot for the change of peak intensity for the starting CuO phase as a function of time under isothermal conditions (200, 230, and 250 °C) is shown in Figure 2b. As in the case of Cu_2O reduction, an induction period is seen. The graph shows that the reduction rate becomes slow and the induction period long with decreasing temperature. Figure 3 displays Arrhenius plots for the reduction rates of CuO and Cu_2O. The apparent activation energy of CuO is about 14.5 kcal/mol, while the value is 27.4 kcal/mol for Cu_2O. Under the conditions of Figures 1 and 2, *the reduction of CuO is easier than the reduction of Cu_2O*. Because of this fact, Cu_2O is probably not seen during the reduction of CuO.

A Rietveld analysis[28,29] was used to calculate phase fractions, lattice constants, and oxygen occupancies from the XRD data obtained under similar conditions at a higher Q (>10 Å^{-1}). The main results of the Rietveld refinement are the following: (1) the data were well fitted with only diffraction lines for CuO and Cu and did not require any other phases, (2) the oxygen occupancy did not vary more than 15% throughout the reduction process, and (3) initially there was a small expansion in all the lattice constants and cell volume of CuO (see Figure 4). These observations are puzzling and suggest that most of the system does not undergo a uniform sequential reduction (bottom of Figure 5). The reduction process could take place mostly in the interface between Cu aggregates and a "sea" of CuO (top of Figure 5). When the relative fraction of Cu becomes dominant (>50%), the metallic copper would start to coat the remaining CuO. As we will see in section III.3, the initial expansion of all the axes in the unit cell of CuO (Figure 4) is consistent with
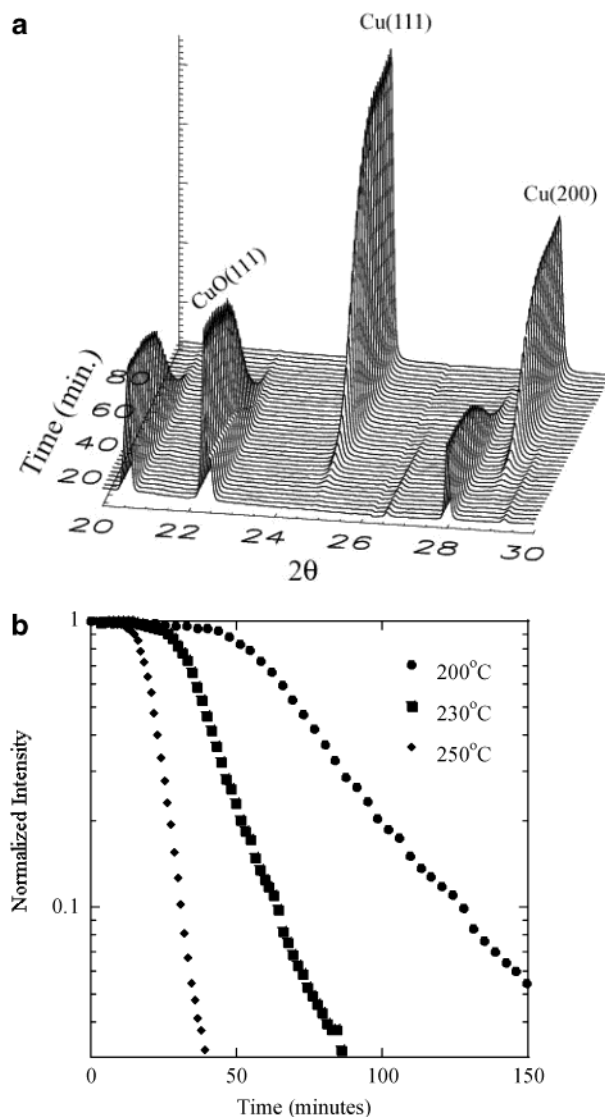
(44) (a) Rodriguez, J. A.; Kim, J. Y.; Hanson, J. C.; Pérez, M.; Frenkel, A. I. *Catal. Lett.* **2003**, 85, 247. (b) Ragone, D. V. *Thermodynamics of Materials*; Wiley: New York, 1995; Vol. I, pp 125−135.
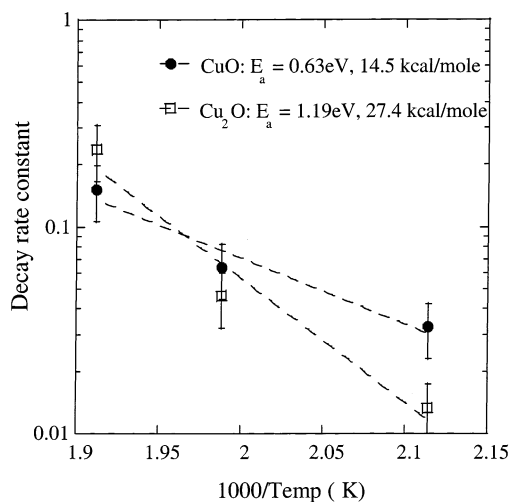

a

Cu(111)

Cu(200)

CuO(111)

Time (min.)

2θ

b

- 200°C
- 230°C
- 250°C

Normalized Intensity

Time (minutes)

Figure 2. Synchrotron-based time-resolved in-situ XRD patterns (λ = 0.9147 Å) during the reduction of CuO by H_2 at constant temperature, 200 °C (a), and changes of CuO (111) peak intensity as a function of time (b). The samples were exposed to a 5% H_2/95% He gas mixture (15−20 cm^3/min flow).

embedding or penetration of some hydrogen into the lattice of the oxide. This expansion cannot be attributed to generation of O vacancies. The decrease in cell volume seen in Figure 4 toward the end of the reduction process is expected for a CuO → Cu transformation.

We found that Cu_2O could be formed as an intermediate in the reduction of CuO after drastically changing the reaction conditions in Figure 2. In a set of experiments the oxide sample was exposed to very small amounts of hydrogen. This increased the temperature for reduction by 50−100 °C and produced Cu_2O as an intermediate. A similar result has been found for the reduction of CuO films under vacuum or high-vacuum pressures of hydrogen.[44] Cu_2O was also detected as an intermediate in TPR experiments with a very large heating rate. Figure 6 shows time-resolved XRD patterns collected near the temperature of appearance of metallic copper when CuO powder is reduced at different heating rates (from 10 °C/min to higher). No hint of an intermediate phase is seen during the reduction when the powder is heated at a rate smaller than 10 °C/min (Figure 6a).

Figure 3. Apparent activation energies for the reduction of CuO and Cu₂O.
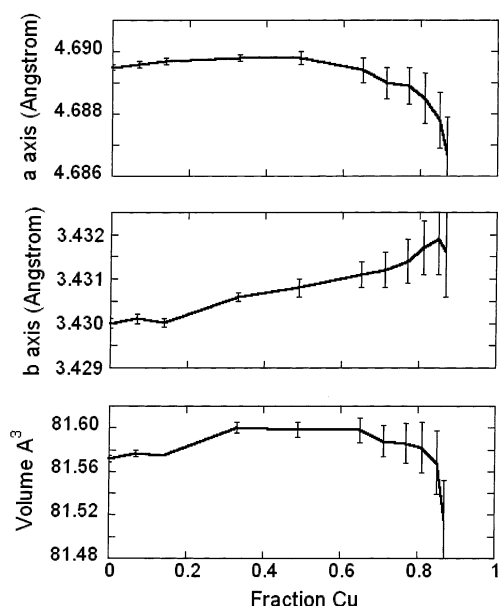

Figure 4. Cell dimensions and volume for CuO as a function of reduction, at 200 °C.
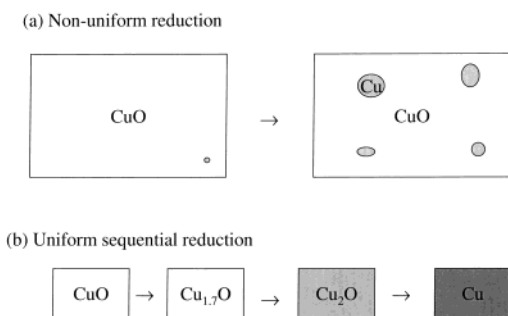

Figure 5. Schematic diagram of two proposed models for the reduction of CuO. Top: In a nonuniform reduction, Cu aggregates start to form around oxide defects on the surface or bulk. The reduction mainly takes place at the Cu−CuO interface. Bottom: Most of the CuO undergoes a sequential loss of oxygen until forming metallic copper.

When the heating rate is increased to 20 °C/min, however, a slight, but clear, hint of Cu₂O phase formation is observed, as indicated by the arrow in Figure 6b. At a higher heating rate (40 °C/min), the existence of the intermediate phase becomes
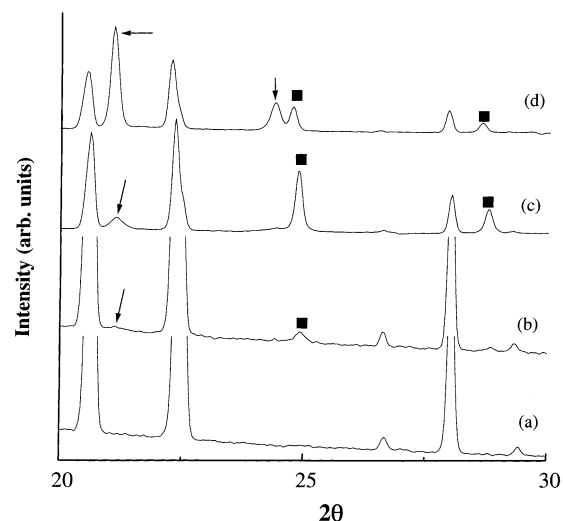
Figure 6. XRD (λ = 0.9147 Å) plots for the formation of Cu₂O phase when CuO powders are reduced at different heating rates: (a) 10 °C/min, (b) 20 °C/min, (c) 40 °C/min, and (d) greater than 50 °C/min. The Cu₂O and Cu peaks are indicated by arrows and solid squares, respectively. The peak intensities are magnified in (a) and (b) to emphasize the intermediate phase.

clear (Figure 6c), and it constitutes nearly 60% in phase fraction when the heating rate is greater than 50 °C/min (Figure 6d). At this large heating rate, the reduction of CuO actually occurs at very high temperatures (>450 °C) when a disproportionation of the type

$$2CuO(solid) \rightarrow Cu_2O(solid) + 0.5\ O_2(gas) \qquad (3)$$
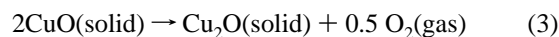
can take place.[44b,45] From a thermochemical viewpoint,[44b] CuO is unstable under very low pressures of O₂ and high temperatures.

III.2. Time-Resolved XANES and EXAFS Studies. Under a normal supply of hydrogen, the time-resolved XRD data show a direct CuO → Cu transformation without a well-ordered intermediate phase. This does not rule out the possible existence of amorphous CuO$_x$ phases. To address this issue, we studied the reduction of the copper oxides with time-resolved XANES/EXAFS.[3,46,47] In agreement with the XRD results, XANES and EXAFS indicate that *the reduction of CuO is easier than the reduction of Cu₂O*. In the XANES data taken at 250, 280, and 300 °C, we found that the changes in the near edge region that occurred during the reduction of both CuO and Cu₂O were dramatic. Typical results are shown in Figure 7. However, based on visual observation only, the presence of an intermediate Cu₂O and/or other Cu$_x$O phases in CuO reduction can be neither confirmed nor ruled out. Figures 8a and 8b show the k^2-weighted EXAFS and Fourier transform magnitudes (uncorrected for photoelectron phase shifts), respectively, of the X-ray absorption coefficient data collected during CuO reduction. The data demonstrate a gradual decrease in the intensity of the lower r peak corresponding to the Cu−O bond in CuO (Figure 8b). This decrease is accompanied by the gradual rise of the higher r peak corresponding to the Cu−Cu first nearest neighbor distance in metallic Cu. After applying the principal component analysis

(45) (a) Rodriguez, J. A.; Hrbek, J. *J. Vac. Sci. Technol. A* **1994**, *12*, 2140. (b) Cotton, F. A.; Wilkinson, G.; Murillo, C. A.; Bochmann, M. *Advanced Inorganic Chemistry*, 6th ed.; Wiley: New York, 1999.
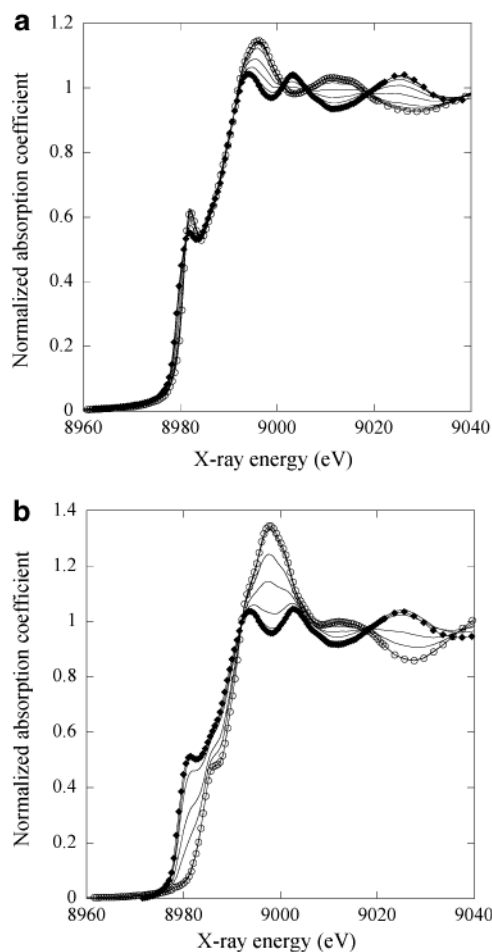(46) (a) Chen, J. G. *Surf. Sci. Rep.* **1997**, *30*, 1.

Figure 7. Plots of time-resolved XANES for (a) Cu_2O and (b) CuO reduction at 300 °C. The open circles correspond to the initial oxides (CuO or Cu_2O), whereas the filled symbols denote the final product (metallic copper).
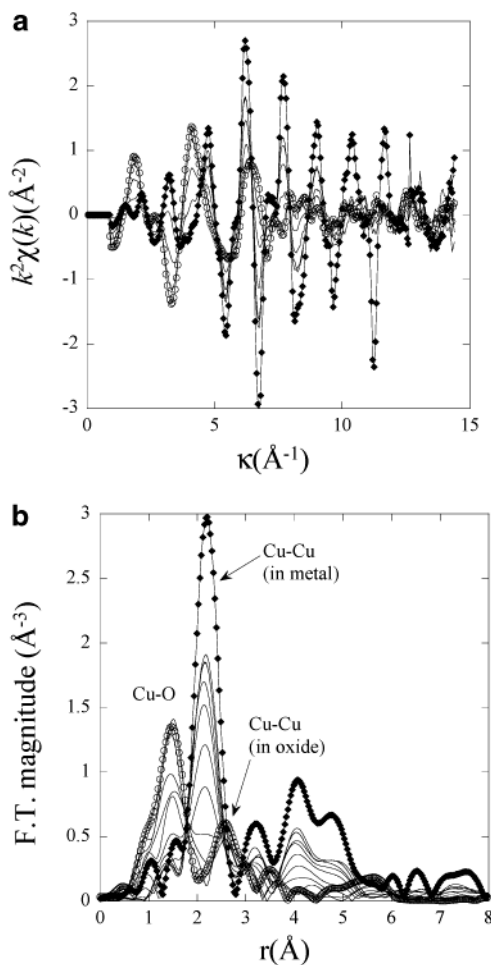

Figure 8. Time-dependent EXAFS spectra in (a) k-space, and (b) r-space for CuO reduction at 250 °C. The open circles correspond to the initial oxides, whereas the filled symbols denote the final product (metallic copper).

(PCA)[22−24] to the series of XANES and EXAFS spectra taken at different temperatures for CuO and Cu_2O reductions, the scree tests demonstrated convincingly that two components (phases) are sufficient to adequately reproduce all the data. Therefore, one would expect that the only two phases that could be present at all times and at all temperatures studied during the Cu_2O and CuO reductions are Cu_2O and Cu, and CuO and Cu, respectively. However, this must be confirmed by quantitative analysis, in which the two components obtained from the PCA analysis of raw XANES/EXAFS spectra are first fit to standard compounds (e.g., metal copper and copper oxides as the most probable species to be found in the data), and if a good fit is obtained, the mixing fraction of these species is then varied to best fit the experimental data collected during reaction. In the case of isothermal Cu_2O reduction, the two components were fit perfectly to (a) pure Cu_2O and (b) pure Cu data measured at the same temperatures, by varying the weighting factors of the components only. This procedure was performed for data taken at all temperatures: 250, 280, and 300 °C. In the case of isothermal CuO reduction, the two components were fit to (a) CuO and (b) Cu data. We would like to emphasize that this method of fitting the principal components to the standard compounds is not model dependent because it is a *linear* fit, and the "wrong" standards can often be ruled out on the basis of the quality of the fits. Because only two independent

components were found in all cases, it was confirmed that the starting phases were reduced to metallic Cu directly, unaccompanied by any intermediate phase formation.
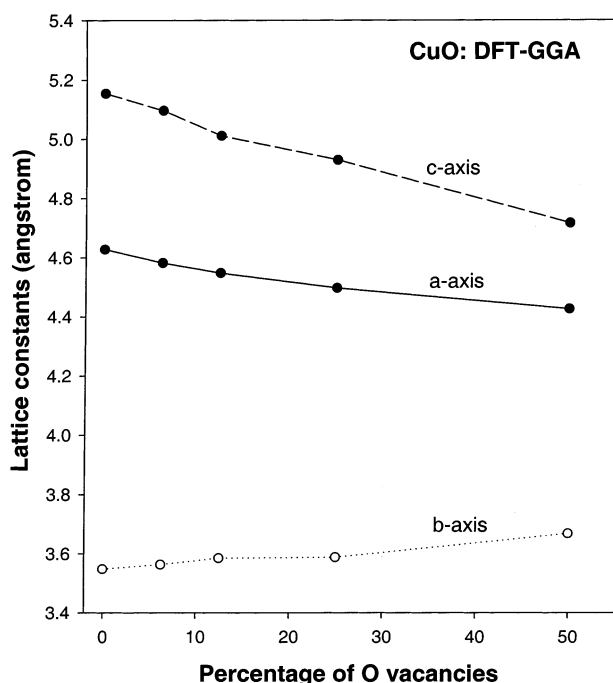
Again, based on the visual observation only, the presence of the intermediate Cu_2O and/or a Cu_xO phase in CuO reduction can be neither confirmed nor ruled out. Indeed, in the cubic (cuprite) and monoclinic (tenorite) crystal structures of both oxides, the average Cu−O distances (which correspond to the lower r peaks at ca. 1.5 Å in the starting phases of the Fourier-transformed EXAFS, Figure 8b, that are not corrected for the photoelectron phase shifts) are close (1.95 Å in CuO versus 1.85 Å in Cu_2O). The average Cu−Cu distances for the both oxide structures are also similar: ca. 3.05 Å (that correspond to the peaks at ca. 2.5 Å in the starting phases of Figure 8b). Therefore, even if a Cu_2O phase were formed during the CuO reduction, its EXAFS features would be peaked in r-space almost at the same positions as the respective CuO features. Their separate structural analyses would thus be strongly model-dependent and less reliable unless statistical techniques such as PCA are used to directly obtain the number of independent species and deconvolute their spectra.

III.3. First-Principles Density-Functional Calculations. On the basis of the XRD and XANES/EXAFS studies described above, one can conclude that under a normal supply of hydrogen the reduction of copper oxide does not follow a sequential

**Table 1.** Calculated Lattice Constants for Copper Oxides and Copper

	cell dimensions	
compound	DFT	exptl
CuO (*C2/c*)	$a = 4.628$ Å	$a = 4.653$ Å[a]
	$b = 3.548$ Å	$b = 3.410$ Å
	$c = 5.154$ Å	$c = 5.108$ Å
	$\beta = 99.52°$	$\beta = 99.50°$
Cu_4O_3 (*I$_1$/amd*)	$a = b = 5.842$ Å	$a = b = 5.837$ Å[b]
	$c = 9.934$ Å	$c = 9.932$ Å
Cu_2O (*Pn-3m*)	$a = b = c = 4.267$ Å	$a = b = c = 4.267$ Å[c]
Cu (*Fm-3m*)	$a = b = c = 3.627$ Å	$a = b = c = 3.615$ Å[c]

[a] From ref 5. [b] From ref 7. [c] From ref 32.

Figure 9. Effects of O vacancies on the lattice constants of CuO. Density functional results.

pathway for a change in oxidation state from "+2" to 0 (i.e., no CuO → Cu_4O_3 → Cu_2O → Cu). Why is this happening? This is not a trivial question since in the oxidation of metallic copper the opposite process to reduction of CuO a sequential pathway is indeed observed (Cu → Cu_2O → CuO).[44,45a,46a] To explain the lack of a sequential reduction, it could be argued that the difference in stability between a CuO system with a large amount of vacancies and the corresponding Cu_4O_3 and Cu_2O phases is not large. We examined this possibility using first-principles DF calculations. Table 1 lists our calculated lattice parameters for CuO, Cu_4O_3, Cu_2O, and metallic Cu. They are in good agreement with experimental measurements.[5–7,32] The DF calculations indicate that the formation of Cu_2O from O_2 and Cu is more exothermic than the corresponding formation of CuO, which is consistent with trends found in the experimental enthalpies of formation for these oxides.[44b]

CuO adopts a monoclinic structure (*C2/c* space group), in which each Cu atom is bonded to four oxygen atoms.[5] The effects of O vacancies on the lattice parameters of CuO are shown in Figure 9. According to the DF results, the presence of O vacancies should induce a substantial increase in the length of the *b*-axis, with a reduction in the length of the *a*- and *c*-axes. Such a progression is necessary to generate the lattice parameters
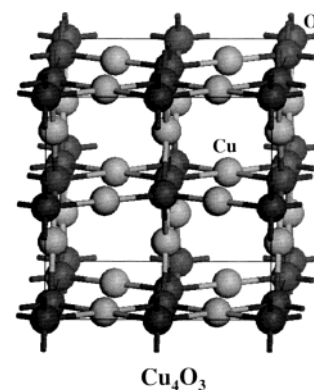
Figure 10. Crystal structure of Cu_4O_3.
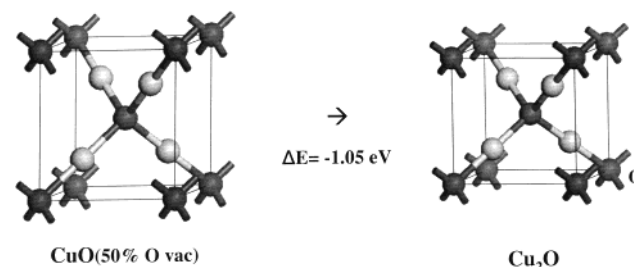
Figure 11. Transformation of CuO (50% O vacancies) into Cu_2O.

of Cu_2O or Cu (see Table 1), but is not observed in the experimental data of Figure 4 when the fraction of CuO is dominant (>50%). At the end of this section, we will explain this discrepancy. A CuO system with 25% of oxygen vacancies was found to be 0.04–0.1 eV/atom less stable than Cu_4O_3 depending on the position of the vacancies within the CuO lattice. Figure 10 shows the crystal structure of Cu_4O_3.[7] It can be seen as a combination of chains of CuO and Cu_2O.[7] Indeed, our DF results show that in this structure half of the Cu cations have a charge similar to that found in CuO, while the charge on the other half of the Cu cations is similar to that of Cu_2O. Thus, Cu_4O_3 appears as an ideal intermediate between CuO and Cu_2O. Although a CuO(25% O vac) → Cu_4O_3 transformation is an exothermic process, it has two major constraints. First, O atoms must be removed in well-defined positions of the CuO lattice. And second, there has to be a substantial distortion in the cell parameters of CuO to obtain Cu_4O_3. From DF results, we estimate that this cell distortion is associated with an activation energy of at least 0.06 eV/atom. Therefore, important kinetic factors probably prevent the formation of Cu_4O_3 as a suboxide or intermediate during the reduction of CuO.

After removing half of the O atoms in CuO in an ordered way (i.e., no random distribution of the O vacancies), one gets a structure in which the arrangement of the atoms can lead to formation of Cu_2O after modification of the cell parameters (see Figure 11). This is an exothermic structural change ($\Delta E \approx$ −1.05 eV/cell or −0.175 eV/atom). We have examined this process in detail using the *b*-axis as reaction coordinate. This is the axis that undergoes the major variation in length when going from CuO (50% O vac) to Cu_2O. Figure 12 displays the calculated energy profile. Points "I" and "F" correspond to the initial and final states in Figure 11, respectively. The "I" point has the original structure of CuO without 50% of the O atoms. After fully relaxing this system, one gets the "A" state. This state is much more stable than the "I" state, but the new
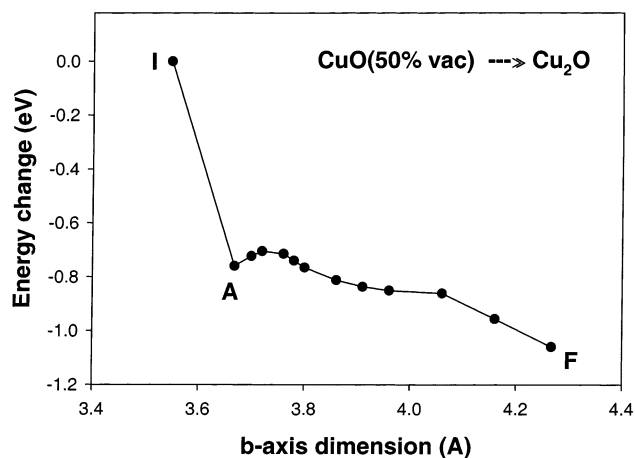
Figure 12. Energy profile for a CuO (50% O vacancies) → Cu₂O transformation as a function of the *b*-axis elongation. In the initial point (I), the system has the crystal structure of CuO with 50% of O vacancies as shown in Figure 11. Full relaxation leads to the "A" state. After this point, the *b*-axis was kept constant at the indicated values while relaxing all the other structural parameters. Point "F" corresponds to Cu₂O.

Table 2. Embedding of H into CuO: Calculated Lattice Constants

stoichiometry	cell parameters (Å)		
	a	*b*	*c*
no H, pure CuO	4.628	3.548	5.154
$Cu_{16}O_{16}H$	4.687	3.591	5.203
Cu_8O_8H	4.836	3.713	5.290
Cu_4O_4H	5.010	3.871	5.506
Cu_2O_2H	5.131	3.965	5.611

crystal structure is still far away from that of Cu₂O. To go from "A" to "F" in Figure 12, we kept the *b*-axis at the indicated values while relaxing all the other structural parameters. Here, to release a relatively small amount of energy (~0.2 eV/cell), the geometry of the system has to change a lot. Furthermore, there is a small activation energy for the "A" → "F" transformation. Thus, the "A" point can be seen as a metastable state. During the reduction of CuO, the system could easily reach "A" and react with hydrogen instead of forming Cu₂O ("F" point) as an intermediate or suboxide. To see the formation of Cu₂O, one has to limit the flow of hydrogen: slow the rate of reduction to allow an "A" → Cu₂O conversion. Indeed, this is what is observed experimentally. In Figure 12, since the "I" and "A" states are less stable than Cu₂O, they should react faster with hydrogen. This can explain why it is easier to reduce CuO than Cu₂O (Figures 1−3). *All these results show the importance of kinetic effects for the formation of a well-defined suboxide during a reduction process.*

The fact that a sequential pathway is observed for the oxidation of metallic copper (Cu → Cu₂O → CuO)[44] is consistent with the kinetic argument described above. The metal sublattice in Cu₂O is similar to that in metallic Cu. The formation for Cu₂O requires only an expansion of the lattice of metallic Cu to make room for the O atoms. On the other hand, to form CuO from Cu, an expansion of the metal lattice and a substantial change of the cell geometry is necessary. Thus, although

$$2Cu(solid) + 0.5O_2(gas) \rightarrow Cu_2O(solid) \qquad (4)$$

$$Cu(solid) + 0.5O_2(gas) \rightarrow CuO(solid) \qquad (5)$$
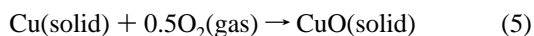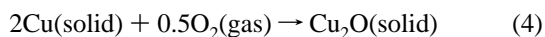
are both exothermic reactions, reaction 4 has a much lower activation energy than reaction 5 and a sequential pathway should be seen for the oxidation of metallic copper.[44,47]

The XRD data in Figure 4 show an expansion of all the lattice constants for CuO during the reduction process. This cannot be attributed to the formation of O vacancies (see Figure 9),

but is characteristic of the penetration or embedding of H atoms in the oxide lattice.[4] Our DFT calculations show that embedded H atoms should expand the lattice of CuO. Table 2 shows the calculated lattice parameters for CuO without hydrogen and with embedded hydrogen ($Cu_{16}O_{16}H$ to Cu_2O_2H stoichiometries). Comparing the lattice expansions in the DF calculations and XRD results, we can estimate that the average concentration of embedded H in the experiments is small (probably $Cu_{16}O_{16}H_{<1}$). The embedded H atoms did not remain in the center of the channels within the CuO structure, but moved toward the O atoms, weakening Cu−O bonds and forming hydroxo-like species. From a Rietveld analysis of our X-ray diffraction data, difference electron density maps show extra electron density at a position consistent with a H in a hydroxo group, but this must be confirmed with future neutron diffraction experiments. Examining the data in Figures 1, 2, and 4, one can conclude that the embedding of H is negligible during the induction time of the reaction and becomes significant at the same time that the reduction rate increases. In the induction time, sites are probably being formed that have a high efficiency for the adsorption and dissociation of H₂.[3,48] Once a significant amount of H is available on the oxide surface, part of it migrates into the bulk of CuO and the formed hydroxo-like species could be precursors for the removal of O atoms as water.

Summary and Conclusions

The reduction mechanism for CuO and Cu₂O by H₂ was investigated in detail. Time-resolved in-situ X-ray diffraction and XANES/EXAFS measurements demonstrated that, under a normal supply of hydrogen, CuO reduces directly to metallic Cu without formation of intermediates or suboxides. The reduction of CuO is easier than the reduction of Cu₂O. The apparent activation energy for the reduction of CuO is about 14.5 kcal/mol, while the value is 27.4 kcal/mol for Cu₂O. During the reduction of CuO, the system can reach metastable states (MS) and react with hydrogen instead of forming Cu₂O. To see the formation of Cu₂O, one has to limit the flow of hydrogen, slowing the rate of reduction to allow a MS → Cu₂O transformation. These results show the importance of kinetic effects for the formation of well-defined suboxides during a reduction process and the activation of oxide catalysts.

The mechanism for the reduction of CuO is complex, involving an induction period and the embedding of H into the bulk of CuO. The higher the temperature, the smaller the magnitude of the induction period. During the induction period sites may be formed for the rapid dissociation of H₂. Then, the migration of H into the bulk of the oxide occurs and the removal of O becomes faster. The XRD data show that most of the system does not undergo a uniform sequential reduction. The

(47) Fernández-García, M. *Catal. Rev.: Sci. Eng.* **2002**, *44*, 59.

(48) Chen, J. G.; Fischer, D. A.; Hardenbergh, J. H.; Hall, R. B. *Surf. Sci.* **1992**, *279*, 13.

reduction process seems to be localized at the interface between Cu and CuO.

JA0301673